Физическая химия

COVALENT DOPING OF g-C$_3$N$_4$ WITH THE BENZO[c][1,2,5]-CHALCOGENADIAZOLE ACCEPTOR BLOCKS: PHOTOCATALYSIS AND ELECTRONIC STRUCTURE

***A.S. Chernukha[1]**, chernukhaas@susu.ru*
***G.M. Zirnik[1]**, glebanaz@mail.ru*
***K.E. Mustafina[1]**, karina040801@gmail.ru*
***N.S. Nekorysnova[1]**, nadin5004@mail.ru*
***A.D. Abramyan[1]**, anton.ma.rum94@gmail.com*
***E.A. Grigoreva[1]**, grigorevaea@susu.ru*
***O.I. Bol'shakov[1,2]**, bolshakovoi@susu.ru*
[1] *South Ural State University, Chelyabinsk, Russian Federation*
[2] *N.D. Zelinsky Institute of Organic Chemistry Russian Academy of Sciences, Moscow, Russian Federation*

The methodology of *in situ* thermal synthesis has been developed for the semiconductors based on graphitic carbon nitride (g-C$_3$N$_4$) doped by benzo[c][1,2,5]chalcogenadiazoles (chalcogen Ch = O, S, Se). Benzo[c][1,2,5]chalcogendiazoles were obtained by methods previously presented in the literature. The purity of the resulting organic structures was confirmed by ^{1}H and ^{13}C NMR, GC-MS, IR-spectroscopy, elemental analysis, and the melting point determination. The technique for obtaining g-C$_3$N$_4$ samples consists in sintering melamine and the required acceptor block mixture at 550 °C in a neutral atmosphere. For pure and doped g-C$_3$N$_4$ its structure formation fact was confirmed by PXRD, IR-spectroscopy and ^{13}C NMR. Semiconductor and other properties of carbon nitride materials were studied by UV-spectroscopy, PL-spectroscopy, cyclic voltammetry technique, SEM conbined with EDS, as well as by plotting nitrogen sorption-desorption isotherms. A series of photocatalytic water-splitting experiments under the UV-light (λ = 365 nm) action in the presence of samples of pure and doped carbon nitride as a photocatalyst, hexachloroplatinic acid as a co-catalyst, and triethanolamine as a electron-sacrificial agent was carried out. The amount of hydrogen formed during the water-splitting experiment was determined for every hour using the GC-method. It was found that all three dopants positively affected photophysical and catalytic properties of the materials. Quantum chemical calculations confirmed that the benzo[c][1,2,5]chalcogenadiazoles served as acceptor blocks with accumulation of the most of the HOMO electron density.

Keywords: carbon nitride, molecular doping, covalent doping, benzochalcogendiazole, acceptor blocks, photocatalysis, water splitting, hydrogen evolution

Introduction

Due to increasing resource and energy demand of the modern society search for energy efficient and resource saving practices becomes priority for the scientific community. The elaboration of semiconductor photocatalysts, with which pure inexhaustible solar energy could be effectively converted, is a promising avenue of sustainable development research. Rediscovery of the carbon nitride in the beginning of the 21 century as a semiconducting photocatalyst boosted the research in the field with fruitful practical and fundamental outcomes. Easy available by simple thermolysis of nitrogen rich precursors carbon nitride is seemed as robust, safe and non-toxic semiconducting platform [1].

Most studied carbon nitride allotrope is generally referred to as a graphitic carbon nitride (g-C$_3$N$_4$) is a polymeric substance consisting of chains with linearly joined in a zig-zag manner heptazine units. These chains are in plane interconnected with hydrogen bonding of residual amino groups and tertiary nitrogens of heptazines. Such structural organization has implications in a typical PXRD graph of g-C$_3$N$_4$ with two major reflexes at 12.8° and 27.7° attributed respectively to the distances between heptazine subunits and polymer chain layers [2].

96

Bulletin of the South Ural State University. Ser. Chemistry.
2022, vol. 14, no. 4, pp. 96–112

Heptazine fragment is a stable and robust heterocycle with sp^2-hybridized carbons and nitrogens. Polymerization of heptazines through secondary aminogroups to linear polymers forms a unique conjugated system of π-electrons with increased charge mobility and reduced bandgap. These particular features of carbon nitride have become a subject of intensive exploitation in the area of photocatalysis, bringing a plethora of examples, alternative to conventionally utilized inorganic photocatalysts.

The molecular origin of g-C₃N₄ allows for the bottom-up construction of various carbon nitride prototypes based on structurally similar to melamine surrogates [3, 4]. g-C₃N₄ layered structure gave rise to various exfoliating approaches leading to the delamination of layers, thus increasing specific surface and electron mobility [5–13]. Delaminated 2D g-C₃N₄ nanosheets exhibit favorable band potentials and exposed active sites, reduced surface defects, increased lifetime of charge carriers, and stronger reduction potential of the photoexcited electrons. Aside from delamination various intercalation techniques provided novel materials with increased charge separation and reactivity [12, 14]. Thermal exfoliation aka thermal oxo-degradation of g-C₃N₄ organic network yields material with an increased specific surface, something that inorganic semiconductors are not capable of [15–17] Another advantage of the semi-organic nature of carbon nitride is the ability to form various nano- and micro-structures based on various types of templating providing a plethora of mesoporous materials with various applications [18, 19].

The purpose of this work is to study the effect of doping of g-C₃N₄ by electron-acceptor blocks, through the introduction of covalently bound benzo[c][1,2,5]chalcogenadiazoles (chalcogen Ch = O, S, Se). For this goal, we are going to obtain the corresponding systems via *in situ* thermal synthesis, to study their photocatalytic activity, and to develop a protocol for simulation the structure and electronic properties on the base of quantum chemical calculations.

We can note that obtaining the experimental information about the structural features of g-C₃N₄ and their changes upon doping by electron-acceptor blocks is a non-trivial and difficult task. However, we can evaluate the trends of structural changes, as well as the factors affecting the electronic properties of the system upon doping, using quantum chemical modeling.

Experimental

Melamine of analytical grade, sulphuric and nitric acid were purchased from Lenreactiv JSC. 1,2-diaminodenzene, hexachloroplatinic acid were purchased from ACROS.

Synthesis of the dopants was accomplished in a two-step synthesis (in Fig. 1), with nitration of starting benzo[c][1,2,5]chalcogenadiazoles, followed by reduction of nitro-group. Synthesis details are described below.
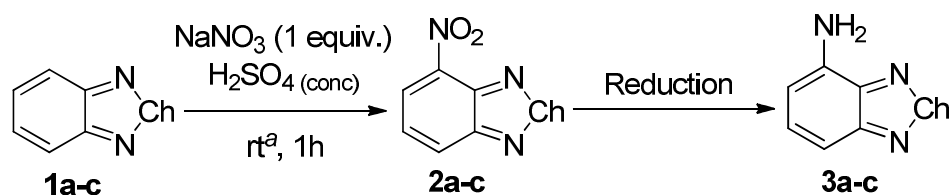

Fig. 1. Synthesis of Benzo[c][1,2,5]chalcogendiazol-4-amines (*Ch* = O, S, Se)

General Procedure for the Synthesis of 4-nitrobenzo[c][1,2,5]chalcogendiazoles (2a-c). In a 100 mL Erlenmeyer flask equipped with a Teflon-coated magnetic stir bar, sodium nitrate (41.6 mmol; 1 eq.) was dissolved in 50 mL of concentrated sulfuric acid. Upon cooling the mixture on an ice bath 1 eq. of benzo[*c*][1,2,5]chalcogendiazole was added so that the temperature of the mixture did not exceed 5 °C. The reaction mixture was stirred at ambient (for benzo[*c*][1,2,5]oxadiazole at 0…5 °C) temperature up to 1 h. until completion (TLC control). Then the reaction mixture was poured into cold water. The precipitate was filtered, washed with water, and dried in a desiccator. The product was used in the next step without purification.

4-nitrobenzo[c][1,2,5]oxadiazole (2a). Yield, 5.29 g (77 %), yellow solid, mp 96–97 °C (93 [20] [lit]). TLC: EtOAc:PE 1:3, R_f, 0.3. ^{1}H NMR (400 MHz, DMSO-d_6) δ 7.86 (dd, J = 9.0, 7.2 Hz, 1H), 8.61 (dd, J = 9.0, 0.7 Hz, 1H), 8.71 (dd, J = 7.2, 0.7 Hz, 1H); MS (EI, 70 eV), m/z (I rel (%)): 165 [M] + (74), 75 (100), 62 (92), 105 (67), 40 (63).

4-nitrobenzo[c][1,2,5]thiadiazole (*2b*). Yield, 5.95 g (79 %), yellow solid, mp 107–108 °C (109 [21] [lit]). TLC: EtOAc:PE 1:3, R_f, 0.5. ^{1}H NMR (400 MHz, DMSO-d_6) δ 7.95 (dd, J = 8.8, 7.5 Hz, 1H), 8.57 (dd, J = 8.7, 1.0 Hz, 1H), 8.68 (dd, J = 7.5, 1.0 Hz, 1H); MS (EI, 70 eV), m/z (I rel (%)): 181 [M] + (100), 123 (78), 151 (68), 64 (64), 135 (58).

4-nitrobenzo[c][1,2,5]selenadiazole (2c). Yield, 8.16 g (86 %), yellow solid, mp 215 °C (227 [22] [lit]). TLC: EtOAc:PE 1:3, R_f, 0.4. ^{1}H NMR (400 MHz, DMSO-d_6) δ 7.76 (dd, J = 8.9, 7.3 Hz, 1H), 8.30 (dd, J = 9.0, 1.1 Hz, 1H), 8.47 (dd, J = 7.3, 1.1 Hz, 1H); MS (EI, 70 eV), m/z (I rel (%)): 228 [M] + (86), 76 (100), 103 (78), 52 (47), 198 (47).

Benzo[c][1,2,5]oxadiazol-4-amine (*3a*). In a 250 mL Erlenmeyer flask was equipped with Teflon-coated magnetic stir bar and a reflux condenser, a 4-nitrobenzo[*c*][1,2,5]oxadiazole (18.2 mmol, 1 eq.) was mixed with concentrated hydrochloric acid (0.145 mol, 8 eq.), SnCl$_2$·2H$_2$O (90.9 mmol, 5 eq.), 70 mL of ethanol, and 30 mL of distilled water. The mixture was stirred at 45…50 °C up to 1 h. until completion of reaction (TLC control). The reaction mixture was cooled to r.t., diluted with water and extracted with DCM (3×50 mL). The organic layer was isolated, washed with NaHCO$_3$ solution and brine, dried over Na$_2$SO$_4$, and concentrated in vacuo. The crude product was purified by flash column chromatography with petroleum ether-ethyl acetate as the eluent.

Yield, 0.79 g (32 %), orange crystals, mp 108–110.5 °C (109–110 [23] [lit]). TLC: EtOAc:PE 1:3, R_f, 0.4. IR, ν/cm^{-1}: 3460, 3360, 3225 (NH), 1635 (NH), 1560, 1530 (C=N-O), 1438, 1390 (N-O), 1315, 1200, 1150, 1000, 889, 875, 845, 785, 730, 685, 615, 595, 530, 475. ^{1}H NMR (400 MHz, DMSO-d_6) δ 7.28 (dd, J = 8.9, 7.3 Hz, 1H), 6.98 (d, J = 8.9 Hz, 1H), 6.52 (s, 2H), 6.31 (d, J = 7.3 Hz, 1H); ^{13}C NMR (100 MHz, DMSO-d_6) δ 150.0, 144.7, 137.1, 135.2, 104.3, 99.6. MS (EI, 70 eV), m/z (I rel (%)): 135 [M] + (100), 51 (36), 52 (35), 78 (28), 117 (27). Anal. Calcd for C$_6$H$_5$N$_3$O: C, 53.33; H, 3.73; N, 31.10; O, 11.84. Found: C, 53.29; H, 3.58; N, 30.57.

Benzo[c][1,2,5]thiadiazol-4-amine (*3b*). In a 250 mL Erlenmeyer flask was equipped with Teflon-coated magnetic stir bar and a reflux condenser, 4-nitrobenzo[*c*][1,2,5]thiadiazole (16.6 mmol, 1 eq.) was mixed with iron powder (58.0 mol, 3.5 eq.), 5 mL of concentrated acetic acid, and 100 mL of distilled water. The mixture was stirred at 55…60 °C up to 2 h. until completion of reaction (TLC control). The reaction mixture was cooled to r.t., diluted with water and extracted with DCM (3×50 mL). The organic layer was isolated, washed with NaHCO$_3$ solution and brine, dried over Na$_2$SO$_4$, and concentrated in vacuo. The crude product was purified by column chromatography with petroleum ether-ethyl acetate as the eluent.

Yield, 1.68 g (67 %), yellow crystals, mp 67–67.5 °C (65.1–66.3 [21] [lit]). TLC: EtOAc:PE 1:3, R_f, 0.6. IR, ν/cm^{-1}: 3355, 3295, 3185 (NH), 1630, 1605, 1545, 1490, 1430, 1370, 1345, 1290, 1275, 1150, 1075, 1020, 960, 900, 875, 850, 835, 800, 740, 610, 565, 515, 475, 460. ^{1}H NMR (400 MHz, DMSO-d_6) δ 7.40 (dd, J = 8.6, 7.4 Hz, 1H), 7.13 (dd, J = 8.7, 0.7 Hz, 1H), 6.58 (dd, J = 7.4, 0.7 Hz, 1H), 6.20 (s, 2H); ^{13}C NMR (100 MHz, DMSO-d_6) δ 155.6, 147.3, 141.0, 132.1, 106.6, 104.8. MS (EI, 70 eV), m/z (I rel (%)): 151 [M] + (100), 124 (22), 92 (16), 66 (9), 152 (9). Anal. Calcd for C$_6$H$_5$N$_3$S: C, 47.66; H, 3.33; N, 27.79; S, 21.21. Found: C, 47.53; H, 3.00; N, 27.70.

Benzo[c][1,2,5]selenadiazol-4-amine (*3c*). In a 250 mL Erlenmeyer flask was equipped with Teflon-coated magnetic stir bar and a reflux condenser, a 4-nitrobenzo[*c*][1,2,5]selenadiazole (13.2 mmol, 1 eq.) was mixed with iron powder (0.105 mol, 8 equiv), ammonium chloride (65.8 mmol, 5 equiv), 80 mL of ethanol, and 20 mL of distilled water. The mixture was stirred at 60…65 °C up to 2 h until completion of reaction (TLC control). The reaction mixture was cooled to r.t., diluted with water and extracted with DCM (3×50 mL). The organic layer was isolated, washed with brine, dried over Na$_2$SO$_4$, and concentrated in vacuo. The crude product was purified by column chromatography with petroleum ether-ethyl acetate as the eluent.

Yield, 0.83 g (32 %), dark-red crystals, mp 153–154.5 °C (159–160 [24] [lit]). TLC: EtOAc:PE 1:3, R_f, 0.4. IR, ν/cm^{-1}: 3345, 3295, 3185 (NH), 3070, 1710, 1630, 1605, 1525, 1490, 1475, 1435, 1380, 1345, 1300, 1280, 1155, 1080, 1015, 960, 865, 800, 735, 605, 515, 470, 430. ^{1}H NMR (400 MHz, DMSO-d_6) δ 7.26 (dd, J = 8.8, 7.3 Hz, 1H), 6.94 (d, J = 8.9 Hz, 1H), 6.35 (d, J = 7.2 Hz, 1H), 6.01 (s, 2H); ^{13}C NMR (100 MHz, DMSO-d_6) δ 160.8, 153.8, 141.8, 132.1, 109.2, 102.9. MS (EI, 70 eV), m/z (I rel (%)): 198 [M] + (7), 92 (100), 119 (97), 199 (75), 197 (38). Anal. Calcd for C$_6$H$_5$N$_3$Se: C, 36.38; H, 2.54; N, 21.21; Se, 39.86. Found: C, 36.29; H, 2.22; N, 21.06.

Synthesis of doped g-C₄N₄ samples

Molecular doping of g-C_3N_4 was considered as an in-situ conjugation of 4-aminobenzo[c][1,2,5]chalcogenadiazol core through side-amino group of heptazine unit with upon thermal treatment of melamine. Melon chain is supposed to be formed simultaneously, with each heptazine unit requiring 2 melamine molecules, according to the scheme. Thus, each doping level 5 would require 5 moles of dopant and (200–2*5) moles of melamine, according to Fig. 2.

Melamine was grinded with corresponding benzo[c][1,2,5]chalcogendiazol-4-amine. The mixture was calcined at 550 °C for 9 h in closed alumina crucible in argon atmosphere. The pristine g-C_3N_4 was obtained similarly, without adding the dopant. Each sample doped with oxygen-, sulfur- and selenium- containing heterocycle was assigned as BODX, BTDX, BSDX, respectively, where X is a doping level in %.
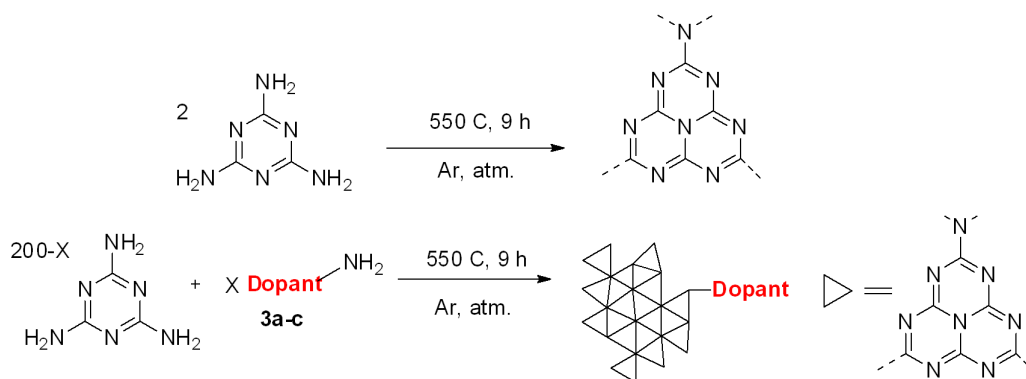

Fig. 2. Stoichiometry of the graphitic carbon nitride formation

Characterization of precursors and carbon nitride samples

Morphology of materials was studied with Scanning electron microscopy (SEM) using JEOL JSM 7001F. Porosity characteristics were evaluated by N_2 adsorption at 77K using an ASAP 2020 Micromeritics apparatus. X-ray diffraction (XRD) patterns were recorded on a Rigaku Ultima IV diffractometer working at Cu Kα radiation (λ = 0.154 nm). A Jeol JEM-2100F transmission electron microscope (TEM) equipped with a field emission gun (FEG) was applied for TEM observations. CHN elemental analysis was performed on a 2400 Elemental Analyzer (PerkinElmer Inc.). Sulfur content was determined with IR-absorption analyzer LECO CS-230. Fourier transform infrared (FTIR) spectra were collected using a Shimadzu IR Affinity spectrometer. UV-spectra recorded with Shimadzu UV-vis 2700 spectrophotometer. The X-ray photoelectron spectroscopy (XPS) measurements were performed using monochromatic X-ray source XM1000 mounted on OMICRON ESCA+ spectrometer (Omicron Nano-Technology, Taunusstein, Germany) with the Al-anode (the radiation energy 1486.6 eV and power 300 W (15 kV, 20 µA)). Photoluminescence spectra of the investigated samples were obtained at ambient temperature with an Shimadzu 6000-RF spectrometer sensitive within 200–900 nm. A 365 nm CW LED laser was employed as the excitation source. ^{1}H and ^{13}C NMR spectra were recorded on a Bruker Avance 600 spectrometer at 400 and 125 MHz respectively. The electrochemical and electrophysical characteristics of the C_3N_4, ABOD, ABSD, and ABTD samples were studied by electrochemical impedance spectroscopy (EIS) using a pulse potentiostat-galvanostat P-40X ("Electrochemical Instruments") with an FRA-24M frequency analyzer. For EIS measurements, a three-electrode electrochemical cell (volume 50 mL) was used. The cell includes a platinum counter electrode, a saturated silver chloride reference electrode (ESR-10101-4.2) and a carbon-paste working electrode (CPE, working surface d = 2 mm, S = 0.0314 cm^2). The material of the working electrode is a paste of the mixture graphene/sample = 50/50 mg/mg and paraffin oil (0.25 mL). The CPE electrode was filled with the test material using a spatula, followed by pressing with a current lead of the working electrode. The electrodes were immersed in a KCl solution (0.05 M), the distance between the electrodes was 1 cm.

Photocatalytic experiment

Photocatalytic decomposition of water with the production of hydrogen in the presence of the sacrificial agent was carried out in accordance with the standard methodology. A weighed portion of carbon nitride (50 mg) was suspended in 35 mL of a 10 vol % aqueous solution of triethanolamine. Plati-

num source, hexachloroplatinic acid (H_2PtCl_6 (aq), 3 wt. % of Pt) was added to the solution. The experiment was carried out in a jacketed quartz reactor isolated from the atmosphere. Before the start of irradiation, the volume inside the reactor was repeatedly evacuated and filled with argon in order to create an inert atmosphere. The reaction mixture was irradiated with UV-light for 5 hours with constant stirring at rt. Periodically, a sample of the gas (1.0 mL) was taken for the analysis. Hydrogen content was analyzed with Crystal-Chromatech 5000 gas chromatograph equipped with thermal conductivity detector. Precise description and layout of irradiation device, are given below.

Irradiation device represented by the 18 pieces of 1W UV-emitting diodes, which have sharp peak of luminosity at 365 nm (Fig. 3) Diodes were mounted closely around the reactor, distance from the source of emission to the surface of reaction solution comprises 1 cm. Precise description and layout of irradiation device presented in Fig. 4.
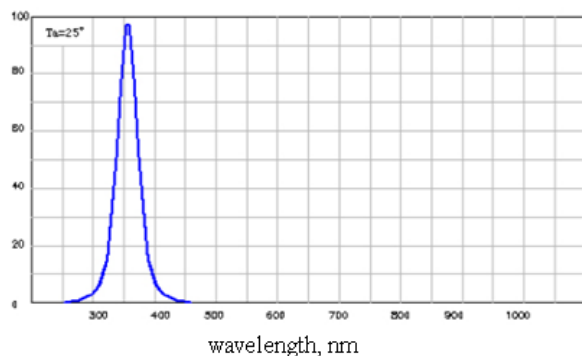

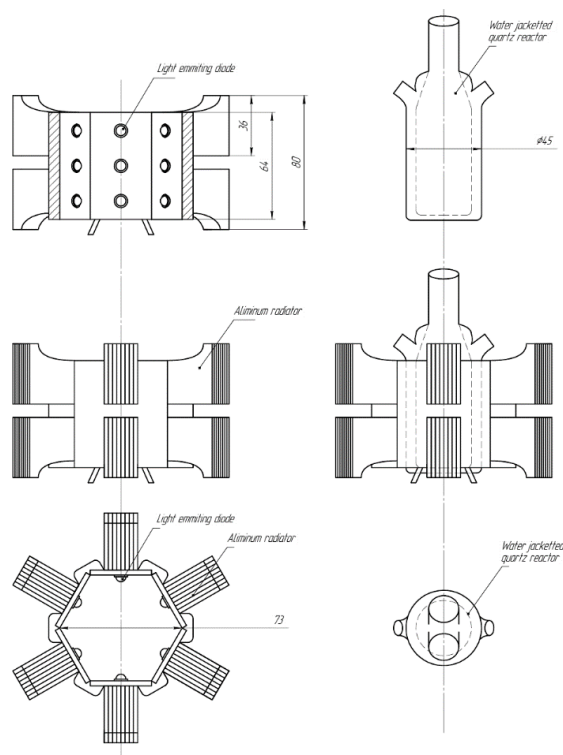**Fig. 3. Luminosity spectrum of the LED, installed in the photoreactor**

Fig. 4. Makeshift photoreactor stand

Apparent quantum efficiency was find according to (1):

$$AQE = \frac{2 \cdot N_{(H_2)}}{I_o \cdot t \cdot V} \cdot 100\% \tag{1}$$

where $N_{(H_2)}$ – amount of hydrogen formed in moles, according (2)

$$N_{(H_2)} = C_{(H_2)} \cdot V. \tag{2}$$

Where $C_{(H_2)}$ – final concentration of hydrogen, V – volume of the photocatalytic reaction, 0.03 L and t – time of the reaction 5*3600 s = 18000 s.

Calculations

The localization of the equilibrium geometry for the pristine melon molecule (M) and for the series of melon structure covalently substituted by benzo[c][1,2,5]chalcogenadiazoles, was performed by DFT methods using Gaussian09 software [25]. The molecular structures were calculated on the B3LYP/6-311+G(d,p) and HSEH1PBE/DGDZVP levels with energy convergence criterion 10^{-8} a.u. The effects of solvation in water were taken into account using PCM [26]. Visualization of calculated structures and analysis molecular orbitals was performed in ChemCraft 1.8 software [27].

100

**Bulletin of the South Ural State University. Ser. Chemistry.
2022, vol. 14, no. 4, pp. 96–112**

Results and discussion

All synthesized samples PXRD peaks appeared at 2θ values of 12.8° and 27.7°, attributed to the (100) and (002) diffraction planes of the typical g-C_3N_4 motif composed of tri-s-triazine building blocks. The most intensive at 27.7 2θ degrees corresponds to the stacking distance 3.20 Å, while the weaker one at 12.8 degrees is the evidence of in-plane regularity with a period of 6.87 Å nm, and is attributed to a melon polymer chain motif [28] (Fig. 5a).

All g-C_3N_4 samples FTIR spectra display three strong bands around 805 cm^{-1}, 887 cm^{-1}, 1100–1700 cm^{-1}, and 3000–3600 cm^{-1}, ascribed to ring-sextant out-of-plane bending vibration of triazine units, the characteristic bending vibration of tri-s-triazine units [29], the stretching mode of aromatic CN heterocycles, and the N-H stretching vibration, respectively [30] (Fig. 5b). NMR spectra of the sulfuric acid dissolved carbon nitride samples are presented in Fig. 5c. All ^{13}C peaks matches previously reported spectra of g-C_3N_4 [31]. Three peaks at 152–160 ppm correspond to a heptazine corner atoms of melon and four peaks at 142–146 ppm are denoted to the bay atoms.
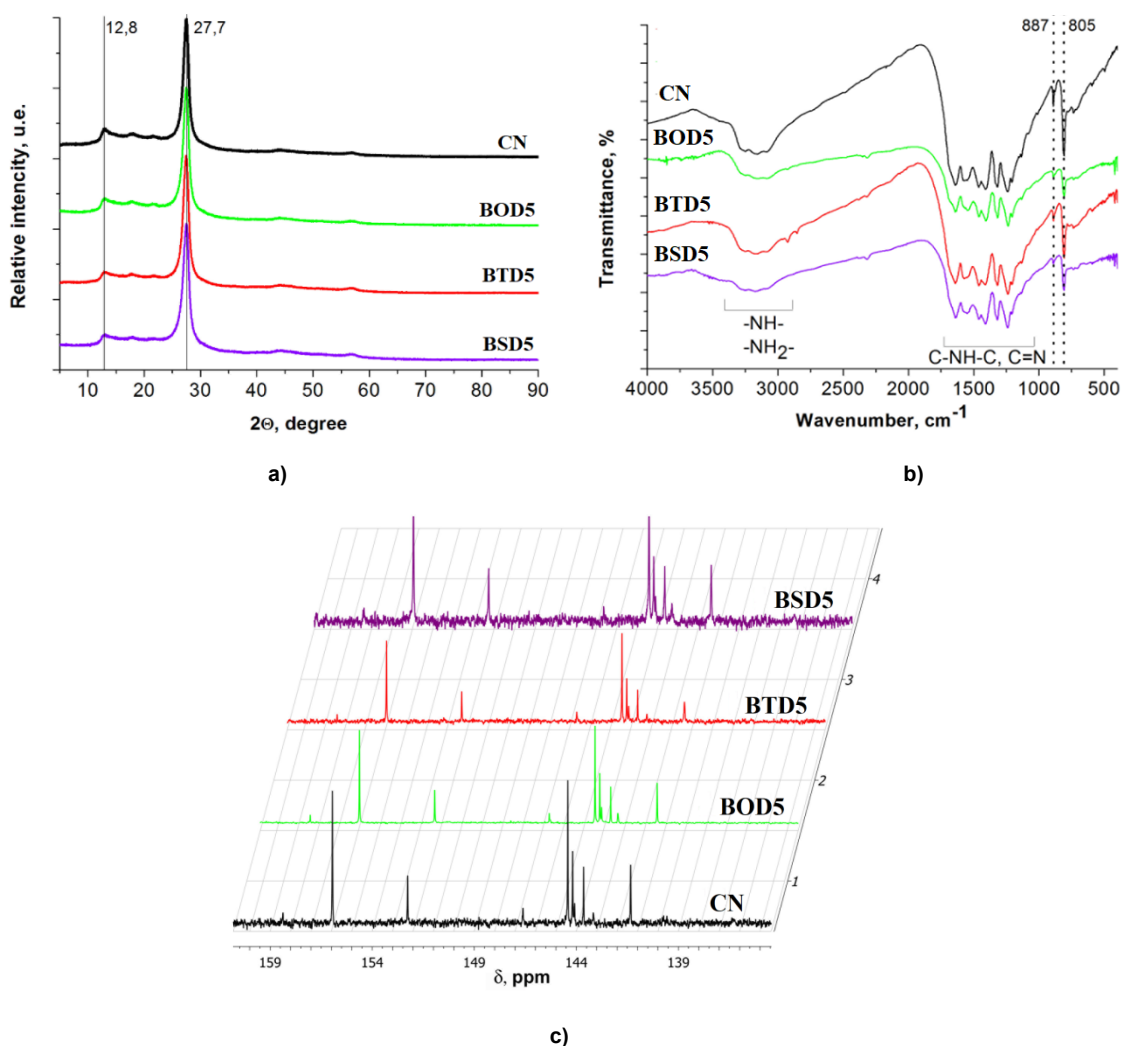

a)

b)

c)

Fig. 5. Spectra of pristine carbon nitride and carbon nitride doped with 4-amino benzo[c][1,2,5]chalcogenadiazoles: a) PXRD; (b) FTIR; c) ^{13}C NMR (where CN = pure C_3N_4; BOD5 = C_3N_4 doped by 5% BOD; BTD5 = C_3N_4 doped by 5% BTD; BSD = C_3N_4 doped by BSD)

SEM microscopy did not reveal significant morphological differences between carbon nitride batches. Samples presented rock-like morphology without a certain pattern or hierarchical structure. Heteroelemental doping was confirmed with SEM EDS microscopy (Fig. 6) with even distribution of chalcogens. Specific surface measured in all three series of samples slightly deviated from average value of 30 m^2·g^{-1} for pristine g-C_3N_4.
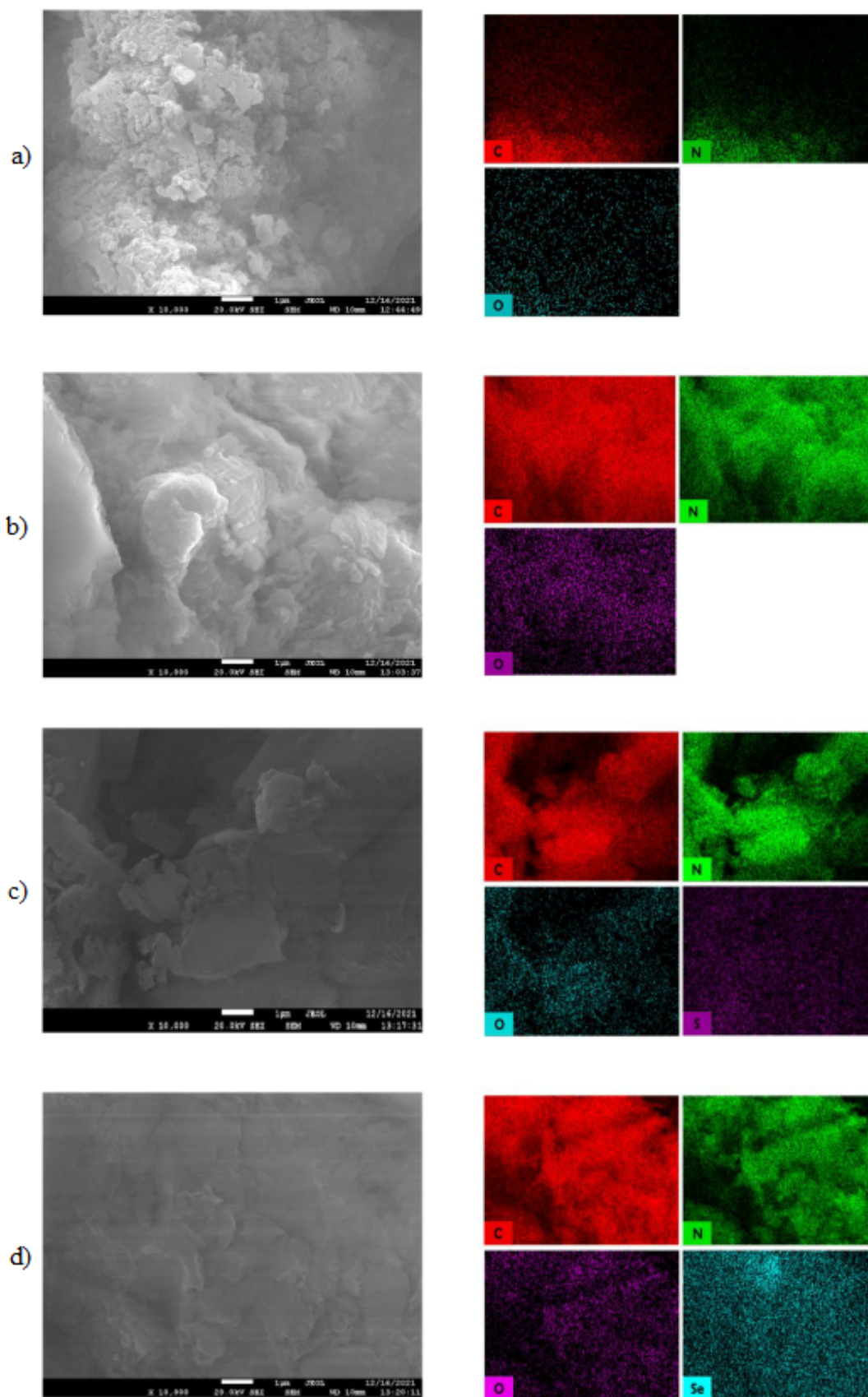
Fig. 6. SEM microphotographs and elemental mapping of the pristine carbon nitride (a), BOD5 (b),
BTD5 (c), BSD5 (d)

102

**Bulletin of the South Ural State University. Ser. Chemistry.
2022, vol. 14, no. 4, pp. 96–112**

Optical properties and photocatalytic activity of pristine and doped g-C₃N₄

Optical properties of g-C_3N_4, including bandgap and optical absorption, were characterized to evaluate its capability of harvesting and utilizing visible photons. g-C_3N_4 is an indirect bandgap photocatalyst, UV-spectra of carbon nitride samples doped at 5 % level, presented in Fig. 7a and Fig. 7b show major absorption cutoff below 450 nm. Heteromolecular doping significantly widened the absorption spectrum. The major absorption edge was considered for the bandgap calculation.[32, 33]. Pristine carbon nitride bandgap values are close to the previously identified bandgap (2.7 eV [34]), whereas doping with oxygen, sulfur and selenium containing heterocycles lowered bandgap down to 2.41, 2.00 and 1.88 eV, respectively.

a)

b)

c)
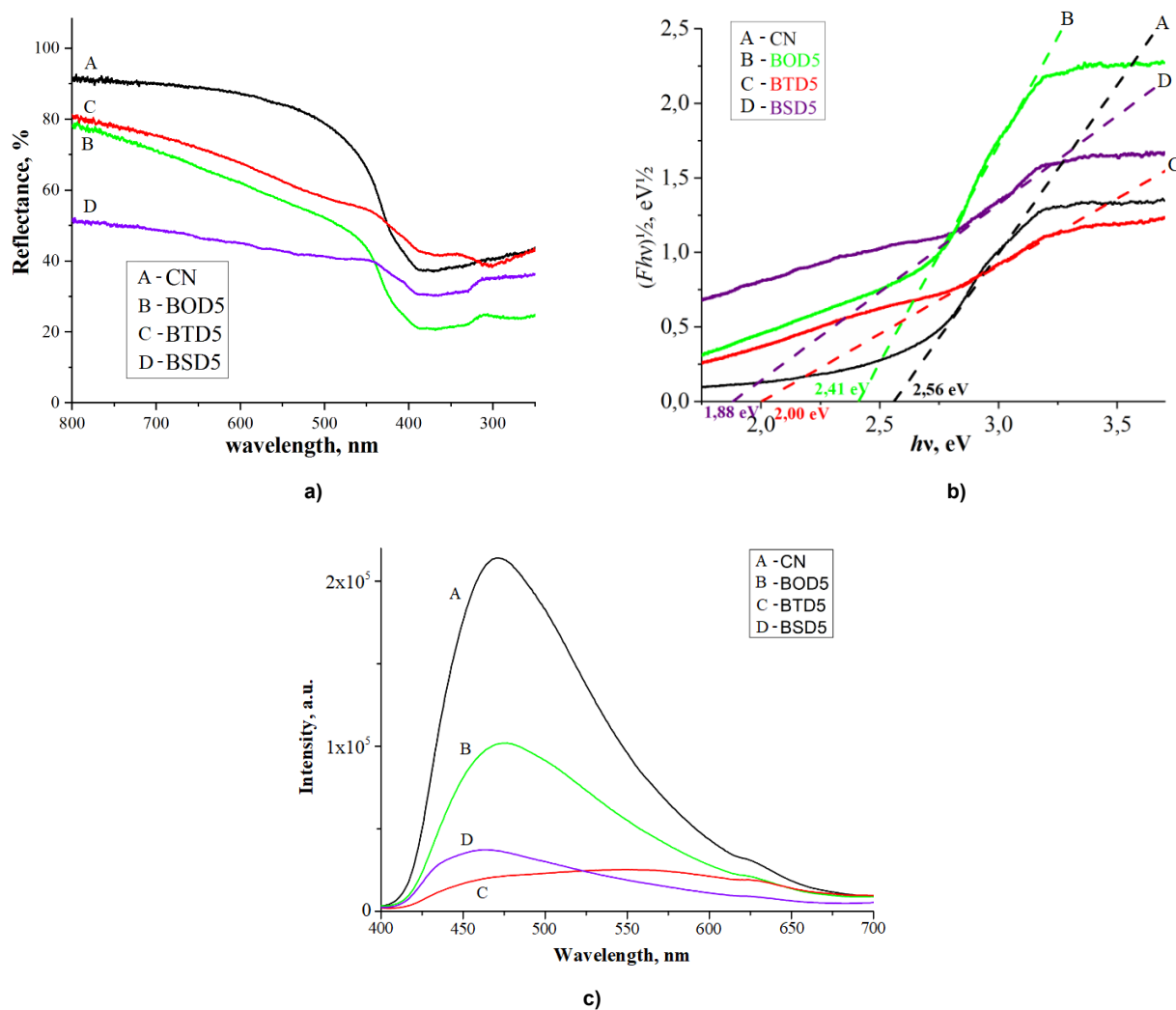
Fig. 7. UV-reflectance spectra (a), Tauc plot (b) and PL-spectra (c) of the doped samples
(where A = pure C₃N₄; B = C₃N₄ doped by 5% BOD; C = C₃N₄ doped by 5% BTD; D = C₃N₄ doped by 5% BSD)

Improved charge separation may enhance the photocatalytic activity of g-C_3N_4 because of an increased amount of charge carriers for photocatalytic reactions. Room temperature photoluminescence (PL) spectra depicted in Fig. 7c show a significant difference in radiative recombination of photoseparated charge carriers in pristine carbon nitride and doped samples. Stabilization of charge carriers is important for heterogeneous photocatalytic reactions as it facilitates their migration to the surface. Benzo[c][1,2,5]thiadiazole doped sample demonstrated the best charge stabilization among chalcogens.

Electrochemical Mott–Schottky plots of carbon nitride and doped samples show typical n-type character (Fig. 8a). The obtained flat band potentials and bandgap energies provide the band structures (Fig. 8b). The levels of the band potentials were calculated relative to the potential of a standard hydrogen electrode (SHE) and vacuum. Molecular doping with 4-aminobenzo[c][1,2,5]chalcogenadizoles almost did not affect the LUMO level, and so the most of the bandgap shortening occurred due to HOMO level upshift.
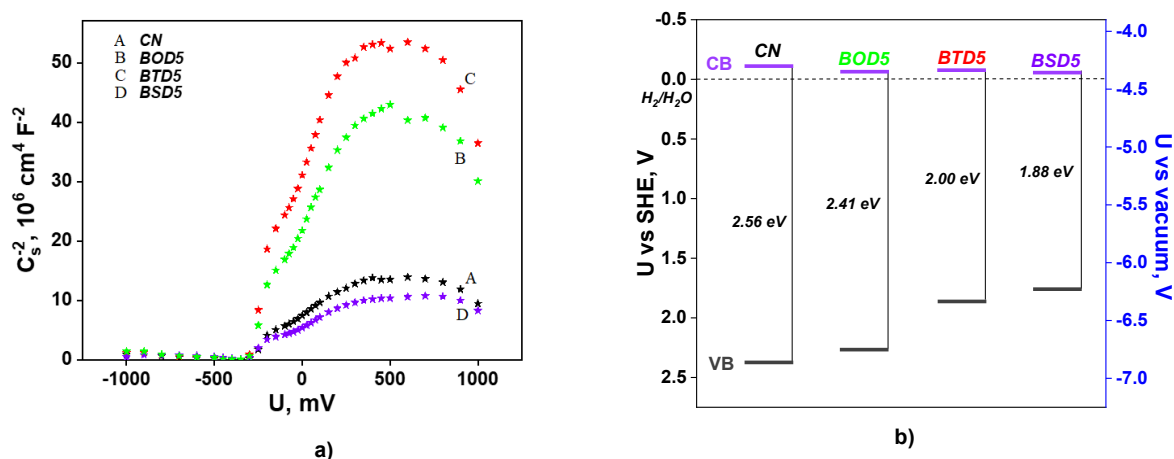
Fig. 8. Mott-Schottky plot (a) and energy band diagrams (b) for g-C₃N₄, BOD5, BTD5 and BSD5 versus vacuum scale and standard hydrogen electrode (where A = pure C_3N_4; B = C_3N_4 doped by 5% BOD; C = C_3N_4 doped by 5% BTD; D = C_3N_4 doped by 5% BSD)

Hydrogen evolution rates in the photocatalytic reaction of water splitting on the pristine carbon nitride and its doped derivatives are given in Fig. 9, where sample modified with benzo[c][1,2,5]selenadiazole demonstrates superior activity. This high hydrogen productivity is in agreement with the bandgaps developed upon molecular doping. A somewhat surprising suppression of photocatalytic activity is also observed for the samples doped with the oxa- and thia-derivatives. Derived hydrogen evolution rate for BSD5 was found to be 72 μmol/h. This level of hydrogen production is below previously reported maximum production (see Table 1) and require further development to optimize electronic structure of the photocatalytic material.
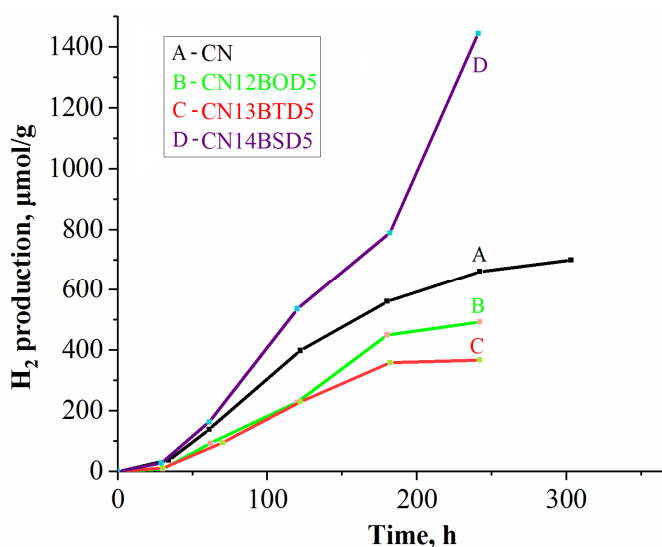

Fig. 9. Photocatalytic hydrogen evolution

Table 1

Hydrogen evolution rates for various catalysts based on molecular doped carbon nirtide

Hydrogen evolution rate, μmol*h⁻¹	Weight of the catalyst, mg	Ref.
131	100	[35]
226	100	[36]
278	100	[37]
29,4	100	[38]
317	100	[39]
229	100	[40]

104

**Bulletin of the South Ural State University. Ser. Chemistry.
2022, vol. 14, no. 4, pp. 96–112**

Table 1 (end)
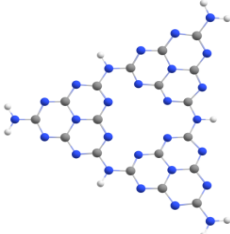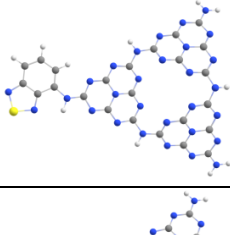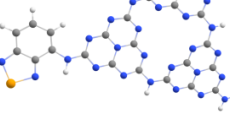
Hydrogen evolution rate, μmol*h⁻¹	Weight of the catalyst, mg	Ref.
31	20	[41]
15	50	[42]
535	50	[43]
106.2	100	[44]
436	100	[45]
31	50 **(A – CN)**	This work
25	50 **(B – BOD)**	
18	50 **(C – BTD)**	
72	50 **(D – BSD)**	

Calculated structural and electronic features of pristine and doped g-C₃N₄

We chose the fragment consist of three heptazine units, which initially has a flat structure, for the simulation of isolated melon molecule and its doped derivatives. The frontier molecular orbital's energy differences (ΔEG) for isolated melon molecules substituted by one of benzo[c][1,2,5]chalcogenadiazoles are given in the Table 2.

Table 2

Calculated properties for doped g-C₃N₄ structures and experimental bandgap values, $BG_{5\%}$

№	Name of compound	Fragment of molecular structure	ΔEG, eV	E(HOMO), eV	E(LUMO), eV	$BG_{5\%}$, eV
0	M/non dopant		3.57	–6.32	–2.75	2.56 (2.70*)
1	BOD/benzo[c][1,2,5] oxadiazole		3.23	–6.40	–3.16	2.41
2	BTD/benzo[c][1,2,5] thiadiazole		3.13	–6.23	–3.10	2.00
3	BSD/benzo[c][1,2,5] selenadiazole		2.93	–6.13	–3.20	1.88

* Experimental BG, according to [34].

Electron-acceptor dopants based on benzo[c][1,2,5]chalcogenadiazoles replace the H atom of the primary amino group, i. e. locate in one of the vertices of the heptazine ring of M, while being in the

same plane with the bound heptazine fragment of melon. The pseudo planar arrangement of these fragments is associated with the effects of conjugation between the dopants and the heptazine ring, which is supported by the possible formation of N…H–C hydrogen bonds (Fig. 10).
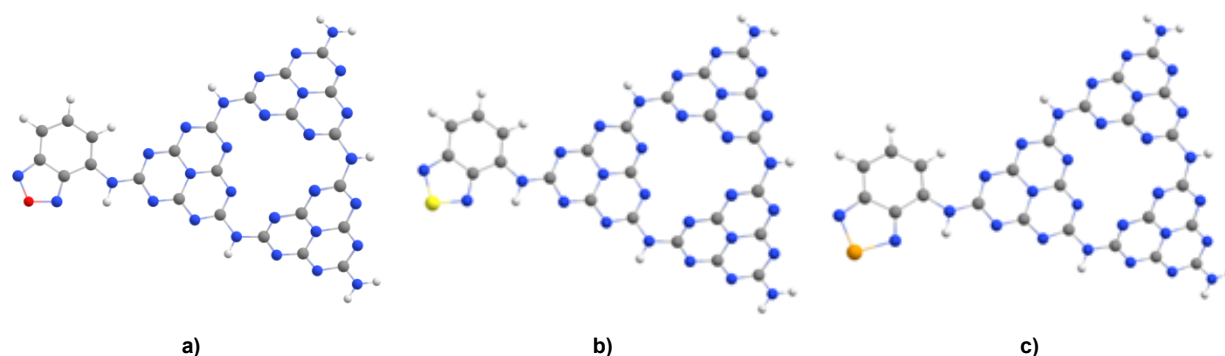

Fig. 10. Optimized doped melon structure with benzo[c][1,2,5]chalcogenadiazoles:
Ch = O (a), Ch = S (b) and Ch = Se (c)

The degree of planarity or the atomics protrusion was determined as the maximum deviation of atomic positions that make up the melon fragment, along the Z coordinate from the XY M-plane. Planarity of the melon molecule is a substantial prerequisite for a full p-electron overlapping in delocalized system. Recent report on differently distorted carbon nitride molecular models demonstrated a planar system having the lowest bandgap [46], Fig. 11a shows a linear relationship between the differences frontier orbital's energies and the degree of planarity of the systems, $r^2 = 0.99$. For an undoped melon molecule, the maximal atomic bulging from the M-plane is 2.35 Å. Melon molecules doped with electron-acceptor units containing benzo[c][1,2,5]chalcogenadiazoles in their structure are flatter that pristine melon, particularly with Ch = Se as the best flattening dopant. Noteworthy, that the models of covalently doped melon, constructed taking into account the effect of the solvent (PCM model), have a less flat structure. In these cases, the atomics protrusion from the M-plane increases by 0.02 Å on average (Fig. 11b).
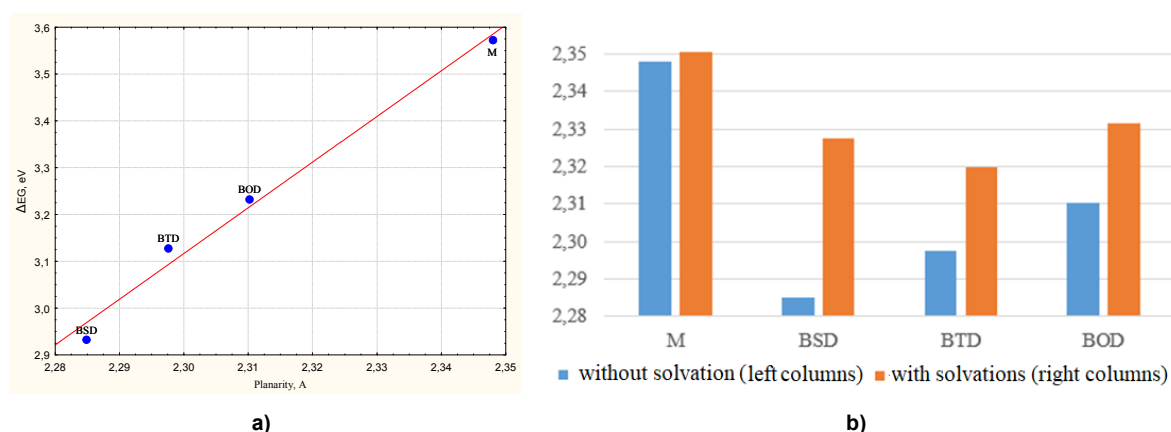

Fig. 11. a) Correlation between the differences frontier orbital's energies, ΔEG and the degree of planarity of systems;
b) Planarity, or out of M-plane atom bulging (in Å) for melon molecule and its covalently doped analogs
with and without solvation

Modification of the structure with any dopants naturally affects the change in the E_{HOMO} and E_{LUMO}. Fig. 12b depicts the energy of frontier orbitals given relatively to the E_{HOMO} of undoped melon, which is equal to – 6.32 eV. Dopant containing benzo[c][1,2,5]selenadiazole, have stronger effect on HOMO and LUMO than those benzo[c][1,2,5]chalcogenadiazoles containing S and O. Overall substitution by electron-acceptor molecules, increases the HOMO level and decreases LUMO level, which is in agreement with previous investigation of similar benzothiadiazole-doped system [34].
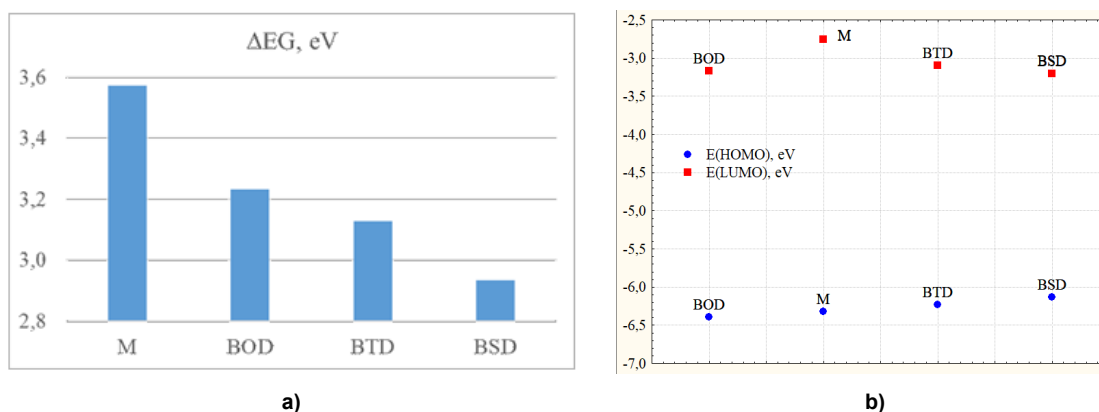
106

Bulletin of the South Ural State University. Ser. Chemistry.
2022, vol. 14, no. 4, pp. 96–112

Fig. 12. a) Energy gap between the HOMO and LUMO, ΔEG; b) Frontier MOs energy

Covalent doping of melon with benzo[c][1,2,5]chalcogenadiazoles molecules localizes HOMO (Fig. 13) mainly on the accepting molecule, and LUMO – simultaneously both on the acceptor fragment and on the joint heptazine fragment. Selenium as an acceptor pulls the electron density of the conjugated electron system onto itself more strongly, increasing the delocalization of electrons, while the polarizability of the system increases and forms planar structures. The maximum flattening of the structures and a change in the configuration of the energy bands leads to a specific localization of the MO's and effective narrows the differences energies between frontier orbital's.
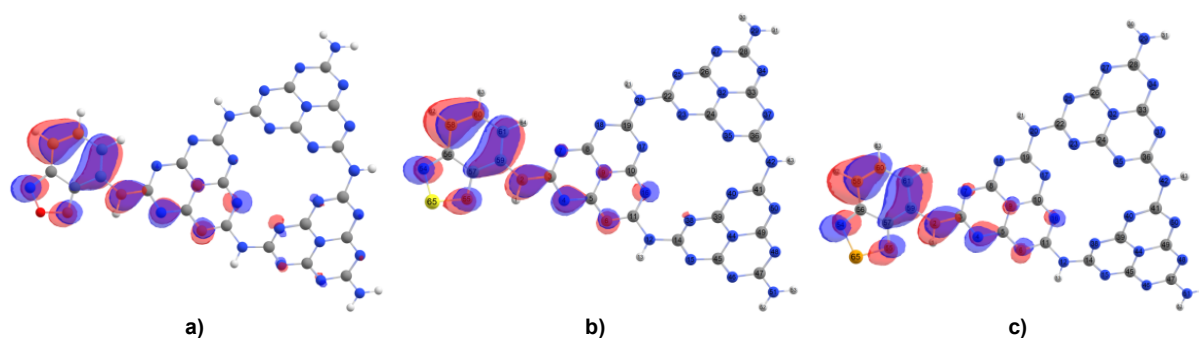

Fig. 13. Localization of HOMO on melon doped by benzo[c][1,2,5]chalcogenadiazoles
a – BOD; b – BTD; c – BSD

In this study, we have continued researches in the area of graphitic carbon nitride electronic structure modification for better photocatalytic performance. Inspired with the burst of organic semiconductor developments driven by donor-acceptor approach, we have introduced three benzo[c][1,2,5]chalcogenadiazoles as acceptors into the carbon nitride scaffold in order to study the effect in a systematic manner. As expected, introduction of the molecular dopants positively affected photophysical properties of the modified materials: it increased the fraction of spectrum absorbed by the material, and stabilized the photo-separated charges. Although selenium-containing dopant shortened bandgap of the carbon nitride better, than other chalcogens, photo-separated charge stability of benzo[c][1,2,5]thiadiazole doped sample was higher.

Although hydrogen production with studied samples of doped carbon nitride showed a somewhat average activity, benzo[c][1,2,5]selenadiazole-doped sample demonstrated superior photoactivity toward hydrogen evolution reaction, possible due to lowest bandgap.

The cluster calculation of the electronic and structural characteristics of the systems under study overestimates the values of differences frontier orbital's energies. The calculated ΔEG and experimental BG$_{5\%}$ values have the same narrowing trend when g-C₃N₄ is modified with benzo[c][1,2,5]chalcogenadiazoles. We have made sure that all considered dopants serves as electron-acceptor blocks localizing most of the HOMO and partially LUMO electron density. Also, ben-

zo[c][1,2,5]selenadiazole was found a geometry improving dopant, as it fixed the planarity of naturally curved melon structure better than other dopants.

References

1. Ong W.J., Tan L.L., Ng Y.H., Yong S.T., Chai S.P. Graphitic carbon nitride (g-C$_3$N$_4$) – based photocatalysts for artificial photosynthesis and environmental remediation: are we a step closer to achieving sustainability? *Chemical Reviews*. 2016;116(12):7159–7329. DOI: 10.1021/ acs.chemrev.6b00075

2. Kessler F.K., Zheng Y., Schwarz D., Merschjann C., Schnick W., Wang X., Bojdys M.J. Functional carbon nitride materials – design strategies for electrochemical devices. *Nature Reviews Materials*. 2017;2:17030. DOI: 10.1038/natrevmats.2017.30

3. See K.A., Hug S., Schwinghammer K., Lumley M.A., Zheng Y., Nolt J.M., Stucky G.D., Wudl F., Lotsch B.V., Seshadri R. Lithium charge storage mechanisms of cross-linked triazine networks and their porous carbon derivatives. *Chemistry of Materials*. 2015;27(11):3821–3829. DOI: 10.1021/acs.chemmater.5b00772

4. Braml N.E., Stegbauer L., Lotsch B.V., Schnick W. Synthesis of triazine-based materials by functionalization with alkynes. *Chemistry – A European Journal*. 2015;21(21):7866–7873. DOI: 10.1002/chem.201405023

5. Xu J., Zhang L., Shi R., Zhu Y. Chemical exfoliation of graphitic carbon nitride for efficient heterogeneous photocatalysis. *Journal of Material Chemistry A*. 2013;1(46):14766–14772. DOI: 10.1039/C3TA13188B

6. Rahman M.Z., Ran J., Tang Y., Jaroniec M., Qiao S.Z. Surface activated carbon nitride nanosheets with optimized electro-optical properties for highly efficient photocatalytic hydrogen production. *Journal of Material Chemistry A*. 2016;(7):2445–2452. DOI: 10.1039/C5TA10194H

7. She X., Xu H., Xu Y., Yan J., Xia J., Xu L., Song Y., Jiang Y., Zhang Q., Li H. Exfoliated graphene-like carbon nitride in organic solvents: enhanced photocatalytic activity and highly selective and sensitive sensor for the detection of trace amounts of Cu^{2+}. *Journal of Material Chemistry A*. 2014;2(8):2563–2570. DOI: 10.1039/C3TA13768F

8. Lin Q., Li L., Liang S., Liu M., Bi J., Wu L. Efficient synthesis of monolayer carbon nitride 2D nanosheet with tunable concentration and enhanced visible-light photocatalytic activities. *Applied Catalysis B: Environmental*. 2015;163:135–142. DOI: 10.1016/J.APCATB.2014.07.053

9. Zhang X., Xie X., Wang H., Zhang J., Pan B., Xie Y. Enhanced photoresponsive ultrathin graphitic-phase C$_3$N$_4$ nanosheets for bioimaging. *Journal of American Chemical Society*. 2012;135(1):18–21. DOI: 10.1021/ja308249k

10. Tong J., Zhang L., Li F., Wang K., Han L., Cao S. Rapid and high-yield production of g-C$_3$N$_4$ nanosheets via chemical exfoliation for photocatalytic H$_2$ evolution. *RSC Advences*. 2015;5(107):88149–88153. DOI: 10.1039/C5RA16988G

11. Cheng F., Wang H., Dong X. The Amphoteric properties of g-C$_3$N$_4$ nanosheets and fabrication of their relevant heterostructure photocatalysts by an electrostatic re-assembly Route. *Chemical Communications*. 2015;5(107):7176–7179. DOI: 10.1039/C5CC01035G

12. Yin Y., Han J., Zhang X., Zhang Y., Zhou J., Muir D., Sutarto R., Zhang Z., Liu S., Song B. Facile synthesis of few-layer-thick carbon nitride nanosheets by liquid ammonia-assisted lithiation method and their photocatalytic redox properties. *RSC Advences*. 2014;4(62):32690–32697. DOI: 10.1039/C4RA06036A

13. Ma L., Fan H., Li M., Tian H., Fang J., Dong G. A simple melamine-assisted exfoliation of polymeric graphitic carbon nitrides for highly efficient hydrogen production from water under visible light. *Journal of Material Chemistry A*. 2015;3(44):22404–22412. DOI: 10.1039/C5TA05850C

14. Xu H., Yan J., She X., Xu L., Xia J., Xu Y., Song Y., Huang L., Li H. Graphene-analogue carbon nitride: novel exfoliation synthesis and its application in photocatalysis and photoelectrochemical selective detection of trace amount of Cu^{2+}. *Nanoscale*. 2014;6(3):1406–1415. DOI: 10.1039/C3NR04759H

108

Bulletin of the South Ural State University. Ser. Chemistry.
2022, vol. 14, no. 4, pp. 96–112

15. Horbett T. Biological activity of adsorbed proteins, in: surfactant science series. *Biology.* 2010;393–413. DOI: 10.1201/9780824747343.ch15.

16. Qiu P., Chen H., Xu C., Zhou N., Jiang F., Wang X., Fu Y. Fabrication of an exfoliated graphitic carbon nitride as a highly active visible light photocatalyst. *Journal of Material Chemistry A.* 2015;3(48):24237–24244. DOI: 10.1039/C5TA08406G

17. Zhao H., Yu H., Quan X., Chen S., Zhao H., Wang H. Atomic single layer graphitic-C₃N₄: fabrication and its high photocatalytic performance under visible light irradiation. *RSC Advences.* 2014;4(2):624–628. DOI: 10.1039/C3RA45776A

18. Li H., Wang L., Liu Y., Lei J., Zhang J. Mesoporous graphitic carbon nitride materials: synthesis and modifications. *Research on Chemical Intermediates.* 2016;42:3979–3998. DOI: 10.1007/s11164-015-2294-9

19. Lakhi K.S., Park D.-H., Al-Bahily K., Cha W., Viswanathan B., Choy J.-H., Vinu A. Mesoporous carbon nitrides: synthesis, functionalization, and applications. *Chemical Society Reviews.* 2017;46(1):72–101. DOI: 10.1039/C6CS00532B

20. Gaughran R.J., Plcard J.P., Kaufman J.V.R. Contribution to the chemistry of benzfuroxan and benzfurazan derivatives. *Journal of American Chemical Society.* 1954;76(8):2233–2236. DOI: 10.1021/ja01637a063

21. Tobiason F.L. Huestis L., Candler C., Pedersen S.E., Peters P. The polar nature of 2,1,3-benzoxadiazole, -benzothiadiazole, -benzoselenadiazole and derivatives as determined by their electric dipole moments. *Journal of Heterocyclic Chemistry.* 1973;10(5):773–778. DOI: 10.1002/jhet.5570100516

22. Murashima T., Fujita K-i., Ono K., Ogawa T., Uno H., Ono N. A new facet of the reaction of nitro heteroaromatic compounds with ethyl isocyanoacetate. *Journal of the Chemical. Society – Perkin Transaction 1.* 1996;(12):1403–1407. DOI: 10.1039/p19960001403

23. Uchiyama S., Santa T., Okiyama N., Azuma K., Imai K. Semi-empirical PM3 calculations predict the fluorescence quantum yields (φ) of 4-monosubstituted benzofurazan compounds. *Journal of the Chemical. Society, Perkin Transaction 2.* 2000;(6):1199–1207. 10.1039/b000170h

24. Sergeev V.A., Pesin V.G., Kotikova N.M. Investigations of 2,1,3-thia- and selenadiazole s - LXVI. Amination of benzo-2,1,3-selenadiazole and its methyl derivatives with hydroxylamine sulfate in concentrated sulfuric acid. *Chemistry of Heterocyclic Compounds.* 1972;8(3):297–299.

25. 2016. Frisch M.J., Trucks G.W., Schlegel H.B., Scuseria G.E., Robb M.A., Cheeseman J.R., Scalmani G., Barone V., Petersson G.A., Nakatsuji H., Li X., Caricato M., Marenich A.V., Bloino J., Janesko B.G., Gomperts R., Mennucci B., Hratchian H.P., Gaussian, (2016).

26. Tomasi J., Mennucci B., Cammi R. Quantum mechanical continuum solvation models. *Chemical Reviews.* 2005;105(8):2999–3093. DOI: 10.1021/cr9904009

27. Zhurko A.G. Chemcraft – graphical program for visualization of quantum chemistry computations, (n.d.).

28. Thomas A., Fischer A., Goettmann F., Antonietti M., Müller J.-O., Schlögl R., Carlsson J.M. Graphitic carbon nitride materials: variation of structure and morphology and their use as metal-free catalysts. *Journal of Materials Chemistry.* 2008;18(41):4893. DOI: 10.1039/b800274f

29. Yang J., Liang Y., Li K., Yang G., Wang K., Xu R., Xie X. One-step synthesis of novel K⁺ and cyano groups decorated triazine-/heptazine-based g-C₃N₄ tubular homojunctions for boosting photocatalytic H₂ evolution. *Applied Catalysis B: Environmental.* 2020;262:118252. DOI: 10.1016/j.apcatb.2019.118252

30. Jin A., Liu X., Li M., Jia Y., Chen C., Chen X. One-pot ionothermal synthesized carbon nitride heterojunction nanorods for simultaneous photocatalytic reduction and oxidation reactions: synergistic effect and mechanism insight. *ACS Sustainable Chemistry & Engineering.* 2019;7(5):5122–5133. DOI: 10.1021/acssuschemeng.8b05969

31. Zhou Z., Wang J., Yu J., Shen Y., Li Y., Liu A., Liu S., Zhang Y. Dissolution and liquid crystals phase of 2D polymeric carbon nitride. *Journal of American Chemical Society.* 2015;137(6):2179–2182. DOI: 10.1021/ja512179x

32. Xue J., Fujitsuka M., Majima T. The Role of nitrogen defects in graphitic carbon nitride for visible-light-driven hydrogen evolution. *Physical Chemistry Chemical Physics.* 2019;21(5):2318–2324. DOI: 10.1039/C8CP06922K

33. Marcì G., García-López E.I., Pomilla F.R., Palmisano L., Zaffora A., Santamaria M., Krivtsov I., Ilkaeva M., Barbieriková Z., Brezová V. Photoelectrochemical and EPR features of polymeric c₃n₄ and o-modified c₃n₄ employed for selective photocatalytic oxidation of alcohols to aldehydes. *Catalysis Today*. 2019;328:21–28. DOI: 10.1016/J.CATTOD.2019.01.075

34. Li K., Zhang W. Creating graphitic carbon nitride based donor-π–acceptor-π–donor structured catalysts for highly photocatalytic hydrogen evolution. *Small*. 2018;14(12):1–12. DOI: 10.1002/smll.201703599

35. Zhang J., Zhang M., Lin S., Fu X., Wang X. Molecular doping of carbon nitride photocatalysts with tunable bandgap and enhanced activity. *Journal of Catalysis*. 2014;310:24–30. DOI: 10.1016/j.jcat.2013.01.008

36. Fan X., Zhang L., Wang M., Huang W., Zhou Y., Li M., Cheng R., Shi J. Constructing carbon-nitride-based copolymers via schiff base chemistry for visible-light photocatalytic hydrogen evolution. *Applied Catalysis B: Environmental*. 2016;182:68–73. DOI: 10.1016/j.apcatb.2015.09.006

37. Zheng D., Pang C., Liu Y., Wang X. Shell-engineering of hollow g-C_3N_4 nanospheres by copolymerization for photocatalytic hydrogen evolution. *Chemical Communications*. 2015;51(47):1–5. DOI: 10.1039/C5CC03143E

38. Zhang J., Chen X., Takanabe K., Maeda K., Domen K., Epping J.D., Fu X., Antonieti M., Wang X. Synthesis of a carbon nitride structure for visible-light catalysis by copolymerization. *Angewandte Chemie. International Edition. A* 2010;49(2):441–444. DOI: 10.1002/anie.200903886

39. Yu Y., Yan W., Gao W., Li P., Wang X., Wu S., Song W., Ding K. Aromatic ring substituted g-c₃n₄ for enhanced photocatalytic hydrogen evolution. *Journal of Material Chemistry A*. 2017;5(33):17199–17203. DOI: 10.1039/C7TA05744J

40. Zhang J., Zhang G., Chen X., Lin S., Möhlmann L., Dołęga G., Lipner G., Antonietti M., Blechert S., Wang X. Co-monomer control of carbon nitride semiconductors to optimize hydrogen evolution with visible light. *Angewandte Chemie – International Edition*. 2012;51(13):3183–3187. DOI: 10.1002/anie.201106656

41. Kailasam K., Mesch M.B., Möhlmann L., Baar M., Blechert S., Schwarze M., Schröder M., Schomäcker R., Senker J., Thomas A. Donor–acceptor-type heptazine-based polymer networks for photocatalytic hydrogen evolution. *Energy Technology*. 2016;4(6):744–750. DOI: 10.1002/ente.201500478

42. Rahman M.Z., Ran J., Tang Y., Jaroniec M., Qiao S.Z. Surface activated carbon nitride nanosheets with optimized electro-optical properties for highly efficient photocatalytic hydrogen production. *Journal of Material Chemistry A*. 2016;4(7):2445–2452. DOI: 10.1039/C5TA10194H

43. Zhang G., Wang X. A facile synthesis of covalent carbon nitride photocatalysts by copolymerization of urea and phenylurea for hydrogen evolution. *Journal of Catalysis*. 2013;307:246–253. DOI: 10.1016/j.jcat.2013.07.026

44. Xu Y., Mao N., Zhang C., Wang X., Zeng J., Chen Y., Wang F., Jiang J.X. Rational design of donor-π-acceptor conjugated microporous polymers for photocatalytic hydrogen production. *Applied Catalysis B: Environmental*. 2018;228:1–9. DOI: 10.1016/j.apcatb.2018.01.073

45. Fan X., Zhang L., Cheng R., Wang M., Li M., Zhou Y., Shi J. Construction of conjugated intramolecular for donor-acceptor copolymers photocatalytic hydrogen evolution, (n.d.) 1–24.

46. Gao Q., Zhuang X., Hu S., Hu Z. Corrugation matters: structure models of single layer heptazine-based graphitic carbon nitride from first-principles studies. *The Journal of Physical Chemistry C*. 2020;124(8):4644–4651. DOI: 10.1021/acs.jpcc.0c00411

110

Bulletin of the South Ural State University. Ser. Chemistry.
2022, vol. 14, no. 4, pp. 96–112

КОВАЛЕНТНОЕ ДОПИРОВАНИЕ g-C₃N₄ АКЦЕПТОРНЫМИ СТРУКТУРАМИ НА ОСНОВЕ 2,1,3-БЕНЗОХАЛЬКОГЕНДИАЗОЛОВ: ФОТОКАТАЛИЗ И ЭЛЕКТРОННАЯ СТРУКТУРА

А.С. Чернуха[1], Г.М. Зирник[1], К.Э. Мустафина[1], Н.С. Некорыснова[1],
А.Д. Абрамян[1], Е.А. Григорьева[1], О.И. Большаков[1,2]
[1] Южно-Уральский государственный университет, г. Челябинск, Россия
[2] Институт органической химии им. Н.Д. Зелинского, РАН, г. Москва, Россия

Разработана методика термического синтеза in situ полупроводников на основе графитоподобного нитрида углерода (g-C₃N₄), допированного бензо[*c*][1,2,5]халькогендиазолами (халькоген Ch = O, S, Se). Бензо[*c*][1,2,5]халькогендиазолы получены ранее представленными в литературе методами. Чистота полученных органических структур подтверждена методами ЯМР ^{1}H и ^{13}C, ГХ-МС, методами ИК-спектроскопии, элементного анализа и установлением точки плавления вещества. Методика получения образцов нитрида углерода заключается в спекании смеси меламина и требуемого акцепторного блока при 550 °C в нейтральной атмосфере согласно специальной программе нагрева. Факт образования структуры для чистого и допированного нитрида углерода был подтверждён методами порошковой дифрактометрии, ИК-спектроскопии и спектроскопии ядерного магнитного резонанса ядер ^{13}C. Полупроводниковые и иные свойства нитридно-углеродных материалов были исследованы методами УФ-спектроскопии, сканирующей электронной микроскопии со вспомогательной функцией рентгеноспектрального микроанализа, спектроскопией фотолюменисценции, циклической вольт-амперометрией, а также методом построения изотерм сорбции – десорбции азота. Проведена серия фотокаталитических экспериментов по разложению воды под действием УФ-излучения (λ = 365 нм) в присутствии образцов чистого и допированного нитрида углерода в качестве фотокатализатора, гексахлорплатиновой кислоты в качестве сокатализатора и триэтаноламина в роли жертвенного агента для поглощения образующихся в ходе реакции «дырок» (h$^+$). Количество образовавшегося в ходе реакции разложения воды водорода определяли с использованием метода газовой хроматографии. Отбор проб производили каждый час. Установлено, что все три допанта положительно влияют на фотофизические и каталитические свойства материалов. Квантово-химические расчеты подтвердили, что бензо[c][1,2,5]халькогендиазолы играют роль акцепторных блоков, накапливающих большую часть электронной плотности ВЗМО.

Ключевые слова: нитрид углерода, молекулярное допирование, ковалентное допирование, бензохалькогендиазолы, акцепторные блоки, фотокатализ, разложение воды, получение водорода

Чернуха Александр Сергеевич – кандидат химических наук, младший научный сотрудник, доцент, кафедра материаловедения и физико-химии материалов, Южно-Уральский государственный университет. 454080, г. Челябинск, проспект Ленина, 76. E-mail: chernukhaas@susu.ru

Зирник Глеб Михайлович – студент, кафедра экологии и химической технологии, Южно-Уральский государственный университет. 454080, г. Челябинск, проспект Ленина, 76. E-mail: glebanaz@mail.ru

Мустафина Карина Эльвировна – студент, кафедра теоретической и прикладной химии, Южно-Уральский государственный университет. 454080, г. Челябинск, проспект Ленина, 76. E-mail: karina040801@gmail.ru

Некорыснова Надежда Сергеевна – студент, кафедра экологии и химической технологии, Южно-Уральский государственный университет. 454080, г. Челябинск, проспект Ленина, 76. E-mail: nadin5004@mail.ru

Абрамян Антон Дмитриевич – студент, кафедра экологии и химической технологии, Южно-Уральский государственный университет. 454080, г. Челябинск, проспект Ленина, 76. E-mail: anton.ma.rum94@gmail.com

Физическая химия

Григорьева Екатерина Алексеевна – кандидат химических наук, доцент, кафедра теоретической и прикладной химии, Южно-Уральский государственный университет. 454080, г. Челябинск, проспект Ленина, 76. E-mail: grigorevaea@susu.ru

Большаков Олег Игоревич – кандидат химических наук, старший научный сотрудник научно-образовательного центра «Нанотехнологии», Южно-Уральский государственный университет. 454080, г. Челябинск, проспект Ленина, 76; Институт органической химии им. Н.Д. Зелинского РАН, 119991, г. Москва, Ленинский проспект, 47. E-mail: bolshakovoi@susu.ru

112

**Bulletin of the South Ural State University. Ser. Chemistry.
2022, vol. 14, no. 4, pp. 96–112**